Laser-Induced Fluorescence Measurements of Mixed Fluid Concentration in a Liquid Plane Shear Layer

M. M. Koochesfahani* and P. E. Dimotakis†
California Institute of Technology, Pasadena, California

The processes of entrainment and mixing are investigated in a nonreacting, uniform density, liquid mixing layer. Laser-induced fluorescence diagnostics and high-speed, real-time digital image acquisition techniques are combined to measure the probability density function of the composition field. Results show that the vortical structures in the mixing layer initially roll up with a large excess of high-speed fluid in the cores. It is found that the mixed fluid composition, above the mixing transition, is essentially uniform across the entire transverse extent of the layer and is asymmetric with a bias in favor of the high-speed fluid. Preliminary observations indicate that the composition of the mixed fluid is more uniform across a liquid shear layer than that in the gaseous layer. The important effect of the resolution capability of the measurement apparatus on the results are discussed and comparisons with recent theoretical calculations are presented.

Introduction

THE majority of the studies on mixing characteristics of turbulent plane shear layers to date have been performed in the gas-phase flows. Results from such studies, both in reacting and nonreacting cases,[1-6] suggest that the entrainment into the fully developed turbulent layer is asymmetric in favor of the high-speed stream. In some cases the distribution of mixture composition has also been measured,[2,22] with conflicting results that will be discussed in due course later in this paper.

By contrast, studies of mixing in liquid mixing layers are few and the fluid composition distribution in this case has, in fact, not been measured. The distinction between gas and liquid, in the context of mixing, arises from their different molecular diffusivities. A gas is characterized by a high mass diffusion coefficient or, in nondimensional form, a low Schmidt number of approximately 0.7, where the Schmidt number, $Sc=\nu/D$, is the ratio of the diffusion coefficient of momentum to that of mass. A liquid has a low mass diffusion coefficient and in the present case of water as the working fluid, $Sc\approx 600$. The study of mixing in the limit of a high Schmidt number—i.e., a liquid—is expected to increase the present understanding of the processes of turbulent transport and mixing and also provides a test bed for the current theoretical models of these processes.

Turbulent transport and mixing were recently investigated[7] in a liquid-phase chemically reacting mixing layer at a moderate Reynolds number corresponding to the early stages of the mixing transition. Even though the results were qualitative, the composition of the mixed fluid was found to be consistent with the entrainment asymmetry. Furthermore, the photographic evidence led to the speculation that this composition could be fairly uniform across the width of the mixing layer.

To quantify these results, a detailed study of the concentration field in a liquid plane mixing layer was undertaken with the primary objective of measuring the distribution of the composition field. The diagnostics were based on laser-induced fluorescence (LIF). A fluorescent dye, which was premixed with the low-speed freestream fluid and diluted by mixing with the high-speed fluid, was used to monitor the relative concentration of high-speed to low-speed fluid in the layer. No chemistry was involved and the dye acted as a conserved passive scalar. The fluorescence intensity was measured along a laser beam, extending across the width of the shear layer, using a 512 element linear photodiode array. In this manner, essentially simultaneous multipoint measurements of species concentration were obtained in the field of illumination with high spatial and temporal resolution. To the extent that a passive scalar technique was used here to measure mixing, these liquid-phase measurements are equivalent to their counterpart in the gas phase.[1,2,22]

Data are presented here at Reynolds numbers both below and above the mixing transition. In the shear layer, the mixing transition is a region corresponding to the introduction of small-scale, three-dimensional motions into the layer.[2,8,9] In the present experiments, the flow parameters required to generate pre- and postmixing transition flows were determined on the basis of Breidenthal's data.[8]

Experimental Facility and Instrumentation

The experiments were conducted in the water mixing layer facility designed by Breidenthal.[8] It is a gravity-driven apparatus in which the freestream fluids are supplied from two independent reservoirs. The low-speed freestream fluid was prepared by adding sodium fluorescein dye to water to a concentration of about 5×10^{-7} M (molar concentration), whereas the high-speed freestream was pure water.

The beam of a 3 W argon ion laser (Coherent Radiation CR-3) was passed through a converging lens to produce a thin beam (diameter in the range of 0.5-1 mm) aligned with the transverse direction of the mixing layer at the midspan position. Variations of the beam diameter along the width of the test section were minimized by using a long focal length lens. The fluorescence intensity along the beam was measured by a Reticon 512 element self-scanning linear photodiode array (see Fig. 1). Even though the reservoir fluids were filtered, scattering of the laser light, mainly at 488 and 514.5 nm, by unwanted particles was observed. An orange photographic filter (Hoya no. 15) effectively blocked any scattered light below 520 nm.

Each element (pixel) of the array receives light from an area in the object plane that is determined by the effective aperture of the pixel (about 25×25 μm) and the magnification ratio of the collecting optics (typically 1:4). This area defines the spatial resolution in the plane of the array and

Presented as Paper 84-0198 at the AIAA 22nd Aerospace Sciences Meeting, Reno, NV, Jan. 9-12, 1984; received Aug. 27, 1984; revision submitted Jan. 20, 1985.

*Research Fellow, Aeronautics. Member AIAA.
†Associate Professor, Aeronautics and Applied Physics. Member AIAA.

for these measurements was given by $\Delta x \times \Delta y \approx 100 \times 100$ μm, where Δx and Δy are the spatial resolution in the flow direction x and the transverse direction y, respectively. The spanwise resolution Δz is determined by the laser beam diameter (see Fig. 2).

Reticon array data were acquired by a computer data acquistion system based on a PDP-11/23 CPU. The output of the array was digitized by a single-channel 8-bit analog/digital (A/D) system capable of 10^7 conversions/s. This A/D system was designed and built in-house by P. Dimotakis, D. Lang, and D. Kerns. The A/D communicates with a DEC Q-bus through a high-speed synchronous bus (D-bus) and a direct memory access (DMA) interface. The D-bus is capable of 12 Mbytes/s and was designed, also in-house, by D. Lang and P. Dimotakis. See Fig. 3 for a schematic of the data acquisition system.

For the experiments reported here, the array was clocked at 640 kHz, which corresponded to a scan time (or temporal resolution) of 0.8 ms and a scan rate of 1250 scans/s. In one case, data were recorded also at 8 ms scan time (64 kHz clock) in order to investigate the effects of degrading the temporal resolution. Two types of data were generally recorded. The first type was acquired at the maximum array clocking rate (i.e., at 640 kHz), stored in the computer memory at that rate, and subsequently recorded on a high-speed disk. In this case, the amount of data, as limited by the system memory, corresponded to 384 scans, each at 512 points across the layer, for a total flow time of 307 ms. This type of data, although suitable for examining the detail structure of the flow, was not sufficient for reliable statistics, since the flow time typically corresponded to the passage of only a small number of large structures.

A second set of data was obtained for statistical purposes by acquiring a long and contiguous data record. Sharing the computer bus cycles between the A/D board and the disk controller, however, limited the fastest rate at which large amounts of data could be digitized and transferred to the disk continuously. To accommodate the maximum data rate, only one out of every eight pixels was digitized, which in effect reduced the transfer rate to 80 kHz without compromising the spatial and temporal resolution of each pixel. With this arrangement, large (up to the disk capacity) amounts of concentration data could be obtained continuously at 64 points across the layer essentially simultaneously. The amount of data per run typically corresponded to the passage of about 100 large structures (approximately 2.5×10^6 numbers).

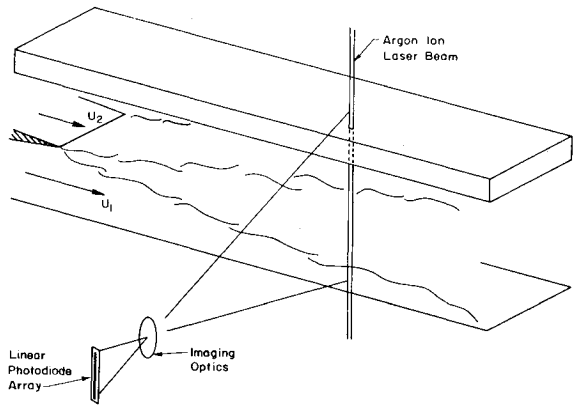

Fig. 1 Optical setup.

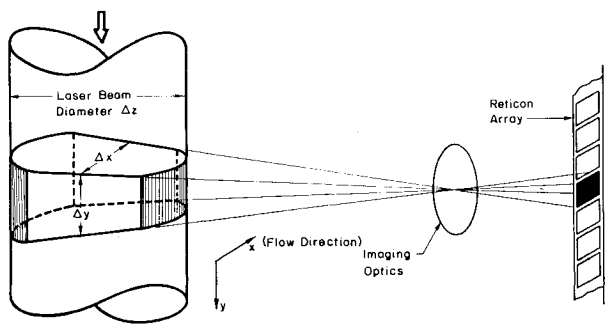

Fig. 2 Schematic of focusing arrangement.

Data Reduction

In this section the steps for converting the raw fluorescence intensity data to high-speed fluid concentration are described.

Computing the Dye Concentration

The output of the ith pixel below saturation, in response to the fluorescence intensity at point y_i along the beam, may be written as[10]

$$V(i) = R(i)\eta[\Omega(i)/4\pi]T_s I_f(i) + D(i) \tag{1}$$

where $V(i)$ is the output voltage, $R(i)$ the pixel sensitivity in V/(J/cm^2), η the optics collection efficiency, $\Omega(i)$ the subtended solid angle, T_s the array scan time, $I_f(i)$ the fluorescence intensity issued from point y_i, and $D(i)$ the dark response.

Note that the photon shot noise has been neglected in Eq. (1) since the typical maximum signal amplitude in the present experiments corresponded to about 6×10^6 photons. The fluorescence intensity I_f is linearly proportional to the local dye concentration C_d and the local laser intensity I and is given by

$$I_f = \alpha C_d I \tag{2}$$

where α is a constant of proportionality determined by the properties of the dye and the optical setup.[10]

The laser intensity is not uniform along the beam and, at a point y_i, can be written as

$$I(i) = I_0(i)\ \exp\left(-\epsilon_0 \int_1^i C_d \mathrm{d}y\right) \tag{3}$$

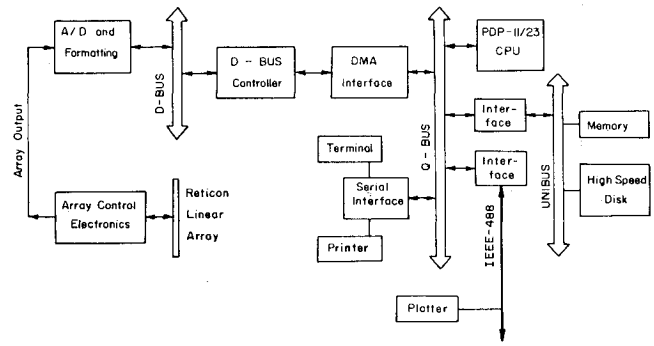

Fig. 3 Schematic of data acquisition system.

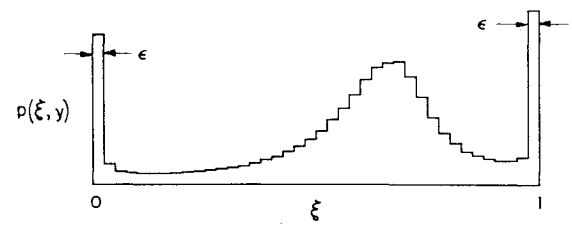

Fig. 4 A typical pdf.

where I is the laser intensity, I_0 the laser intensity in the absence of attenuation, ϵ_0 the dye molar absorption coefficient, and C_d the local molar dye concentration. The first term accounts for the laser intensity variation as established primarily by the converging lens. The second term accounts for the cumulative absorption between a reference point in the freestream, imaged on the first pixel, and point y_i.

Combining Eqs. (1-3) and lumping all of the parameters that are independent of the dye concentration into a single term $\beta(i)$ gives

$$V(i)=\beta(\mathrm{i})\exp\left(-\epsilon_0\int_1^i C_d\mathrm{d}y\right)C_d(i)+D(i) \tag{4}$$

The quantity $\beta(i)$ contains the effects of nonuniformity of imaging and pixel sensitivity, laser beam diameter variation, and possible small misalignments between the array and the beam. It is experimentally measured by recording the fluorescence intensity along the beam resulting from a very dilute uniform dye solution in the test section. $D(i)$ is measured by recording the output of the array with the test section filled with clear water (i.e., no dye present). The approximation

$$\int_i^{i+1} C_d\mathrm{d}y\approx\Delta y C_d(i)$$

reduces Eq. (4) to

$$C_d(i)=\frac{V(i)-D(i)}{\beta(i)}\prod_{j=1}^{i-1}\exp[\epsilon_0\Delta y C_d(j)] \tag{5}$$

To extract the dye concentration at a given point, the instantaneous laser intensity at that point must be known. The laser-beam is attenuated, however, in passing through the dye concentration field that is set up by the flow. One advantage of linear arrays is that each scan of the array contains information at many closely spaced points essentially simultaneously. This, in effect, allows one to perform the operation indicated by Eq. (5) on the data and remove the effects of attenuation and various nonuniformities on a scan-by-scan basis.

Inferring the High-Speed Fluid Concentration

The local instantaneous dye concentration C_d in a sampling volume is given by

$$C_d=C_{d_0}[v_2/(v_1+v_2)] \tag{6}$$

where C_{d_0} is the freestream dye concentration carried by the load-speed fluid, v_2 the volume of low-speed fluid in the sampling volume, and v_1 the volume of high-speed fluid in the sampling volume. The normalized concentration of high-speed fluid ξ is thus equal to

$$\xi=1-C_d/C_{d_0} \tag{7}$$

where $\xi=v_1/(v_1+v_2)$ is defined as the high-speed fluid volume fraction.

Equations (5) and (7) form the basis of calculation of the local instantaneous concentration. Since the whole width of the shear layer is imaged on the array, C_{d_0} is available for each scan making calculation of Eq. (7) relatively simple.

Calculation Based on the PDF

A useful way of studying the concentration field is in terms of its probability density function (pdf). The interest in the pdf stems from the fact that an important approach to the calculations for many problems of practical interest in chemically reacting flows requires the knowledge of the pdf for that flow. This approach is discussed in some detail by Bilger.[11] This section serves to introduce the definitions and properties of the quantities discussed in this work and how they are related to the pdf.

The output of each photodiode of the array results in the measurement of concentration as a function of time $\xi(t)$ at the corresponding imaged point in the layer. Note that ξ is defined in the previous section as the high-speed fluid volume fraction. The probability density function of ξ at a given point y in the layer is denoted by $p(\xi,y)$ and is the fraction of time that $\xi'(t)$ falls inside the range $(\xi,\xi+\Delta\xi)$. Specifically,

$$p(\xi,y)\Delta\xi=\mathrm{Prob}\{\xi<\xi'(t)\leq\xi+\Delta\xi\} \tag{8}$$

for small $\Delta\xi$. In these measurements, the range of ξ was divided into 32 levels so that $\Delta\xi$ was equal to 0.031. Normalization of the pdf requires that

$$\int_0^1 p(\xi,y)\mathrm{d}\xi=1 \tag{9}$$

The average concentration of high-speed fluid $\bar{\xi}$ is then given by

$$\bar{\xi}(y)=\int_0^1 \xi p(\xi,y)\mathrm{d}\xi \tag{10}$$

A typical $p(\xi,y)$ is shown in Fig. 4. The two "delta" functions at $\xi=0,1$ are associated with the pure unmixed fluids of the low- and high-speed sides, respectively. Their widths are dictated by the overall signal-to-noise ratio of the measurement and therefore, are not zero in practice. Concentrations in the range $0\leq\xi<\epsilon$ are assigned to pure (unmixed) low-speed fluid and $1-\epsilon<\xi\leq1$ to pure high-speed fluid. The range $\epsilon\leq\xi\leq1-\epsilon$ would, therefore, correspond to mixed fluid. The value of ϵ was 0.031 [same as $\Delta\xi$ in Eq. (8)]. The mixed fluid pdf (i.e., excluding the two delta functions) may be characterized by its area and first moment as defined below.

The area under the mixed fluid pdf P gives the total probability of finding mixed fluid at *any* concentration. It is given by

$$P(y)=\int_\epsilon^{1-\epsilon} p(\xi,y)\mathrm{d}\xi \tag{11}$$

A value of $P(y)$ less than unity signifies the presence of unmixed fluid. The following two reference quantities were defined based on $P(y)$. The location $y=0$ was arbitrarily chosen to coincide with the point where the total probability of finding mixed fluid was at a maximum [i.e., position of maximum $P(y)$]. A reference thickness δ_1 was defined as the 1% width of the total mixed fluid probability $P(y)$, where P had dropped to 1% of its maximum value. δ_1 was found to agree very well with the visual width of the layer[10] and, therefore, it is referred to here as the layer visual thickness.

The first moment of $p(\xi,y)$, also called the average mixed fluid concentration, is given by

$$C_m(y)=\int_\epsilon^{1-\epsilon}\xi p(\xi,y)\mathrm{d}\xi\Big/\int_\epsilon^{1-\epsilon} p(\xi,y)\mathrm{d}\xi \tag{12a}$$

which can also be written as

$$C_m(y)=\int_\epsilon^{1-\epsilon}\xi p(\xi,y)\mathrm{d}\xi\Big/P(y) \tag{12b}$$

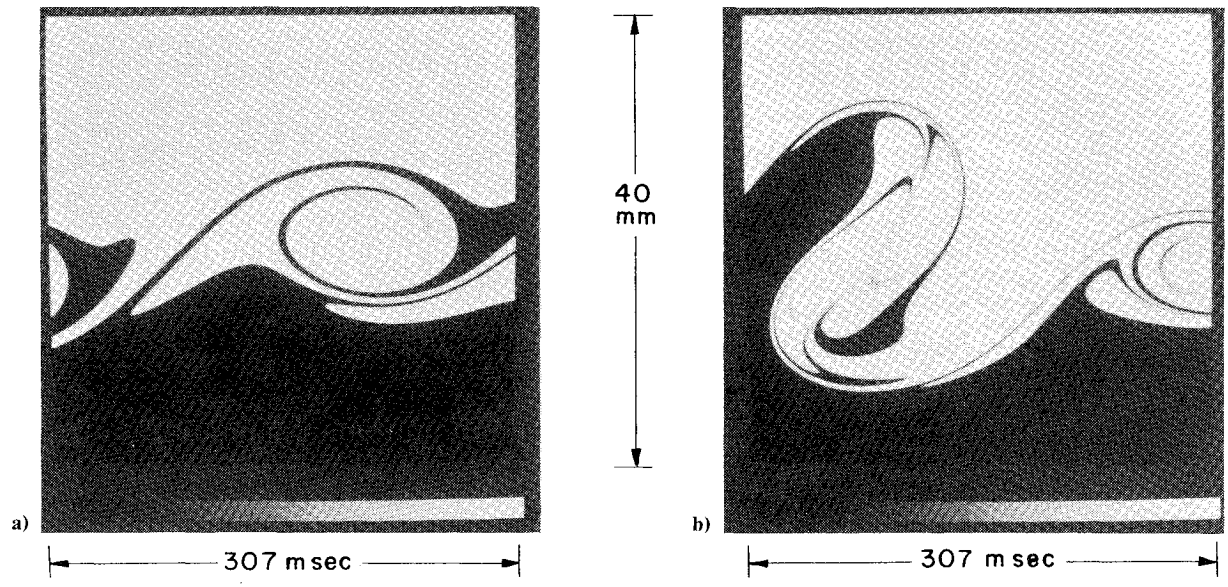

Fig. 5 Digital LIF picture before the mixing transition, $U_2/U_1 = 0.46$, $Re \approx 1750$; a) single vortex, b) pairing vortices.

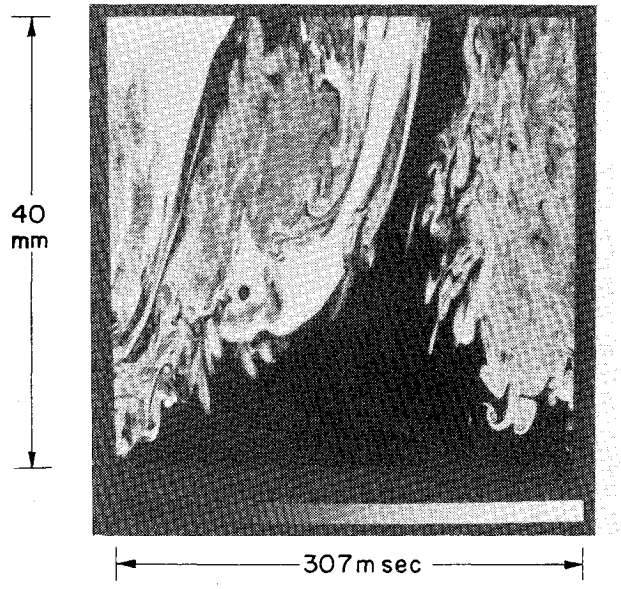

Fig. 6 Digital LIF picture above the mixing transition, $U_2/U_1 = 0.38$, $Re \approx 23{,}000$.

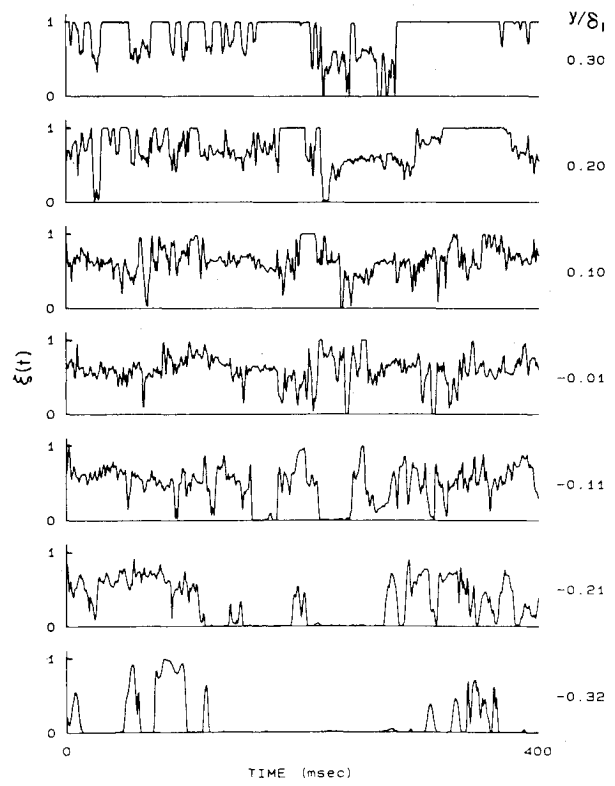

Fig. 7 High-speed fluid concentration vs time above the mixing transition, $U_2/U_1 = 0.38$, $Re \approx 23{,}000$, 0.8 ms scan.

And finally, we define the total mixed fluid concentration for the entire layer by

$$C_M = \int_{-\infty}^{+\infty} P(y) C_m(y) \mathrm{d}y \Big/ \int_{-\infty}^{+\infty} P(y) \mathrm{d}y \qquad (13)$$

Results and Discussion

Results below the Mixing Transition

A sample of the digital LIF data in a plane mixing layer is displayed in Fig. 5. The two photographs, taken from a digital image processing monitor screen, show the concentration field before the mixing transition as defined by Breidenthal.[8] The data were recorded at a downstream distance from the splitter plate of $x = 18$ cm with $U_1 = 13$ cm/s and $U_2/U_1 = 0.46$. The local Reynolds number, based on the local visual thickness δ_1 and the velocity difference ΔU, was $Re = \delta_1 \Delta U/\nu \approx 1750$. Each picture represents 384 successive scans, each at 400 points across the layer, for a total flow time of 307 ms.

It should be emphasized that, technically speaking, these are not "photographs." The vertical extent maps into 40 mm of the transverse coordinate of the shear layer. The horizontal extent is time (increasing from right to left). These y-t pictures were constructed in the computer by transmitting to the image processor, in reverse order, consecutive scans of the array for processing and display. The grey level assignment is such that the intensity varies linearly with ξ, with white corresponding to pure (unmixed) high-speed fluid ($\xi = 1$) and black to pure low-speed fluid ($\xi = 0$) with in-

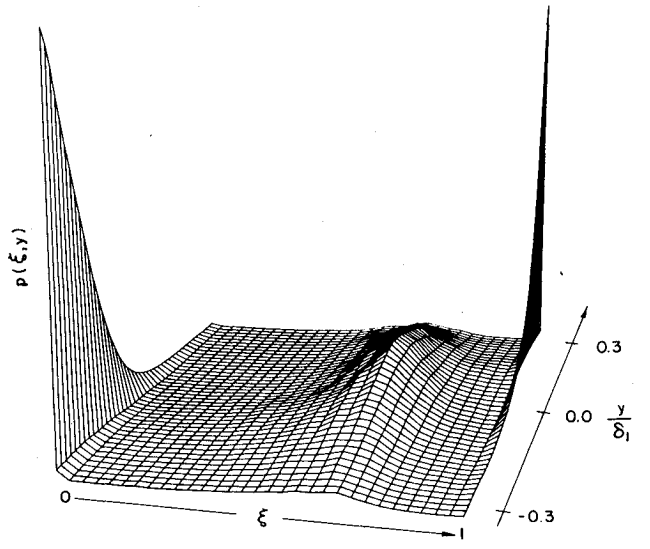

Fig. 8 pdf of the composition field above the mixing transition, $U_2/U_1 = 0.38$, $Re \approx 23{,}000$, 0.8 ms scan.

termediate shades of grey (i.e., $0 < \xi < 1$) indicating mixed fluid.

Figure 5 shows that the concentration field before the mixing transition is rather simple. It consists of pure unmixed fluids originating from either high- or low-speed freestreams. Mixed fluid is found only at the thin interfaces separating the two fluids. The large excess of high-speed fluid in the core of the structures is noteworthy. This result and also measurements at stations closer to the splitter plate[10] indicate that the vortical structures in the mixing layer initially roll up with a large excess of high-speed fluid entrapped in their cores. This behavior seems to have gone mostly unnoticed, even though photographic evidence for it has been available (see, for example, Refs. 1, 12, 13). It must be emphasized that this initial large asymmetry in the core composition is different from and should not be confused with the entrainment asymmetry into the fully developed layer. There is no clear explanation for this phenomenon and, in fact, many calculations of the mixing layer in the past (e.g., see Refs. 14 and 15) have produced symmetric patterns in disagreement with the observations made here.

Results above the Mixing Transition

A *y-t* "photograph" of the composition field above the mixing transition is presented in Fig. 6. It was prepared in the same fashion as Fig. 5. The data were recorded at $x = 25$ cm with $U_1 = 70$ cm/s and $U_2/U_1 = 0.38$. The value of the local Reynolds number was $Re \approx 23{,}000$. The change in the apparent aspect ratio of the large structures is the result of the fixed scanning rate used in these measurements and the increase of the freestream velocities. Figure 6 exemplifies the essential features of the flow in this region. Consistent with previous results,[16-18] it can be seen that the vortical motion of the structure transports fresh fluid from the high-speed side (white) all the way down to the low-speed side (black) and vice versa. The most striking result is the rather uniform composition of the fluid inside the structure, which is more or less of the same shade of grey. There is no tendency toward lighter shades in the neighborhood of the high-speed side or toward darker shades on the low-speed side. These observations are in general agreement with those of Wygnanski et al.[19] in their heated mixing layer (e.g., see their Fig. 7).

Time traces of the high-speed fluid concentration, above the mixing transition, are shown at seven locations across the layer in Fig. 7. Each time trace is composed of 500 consecutive data points connected by straight lines. δ_1 in this

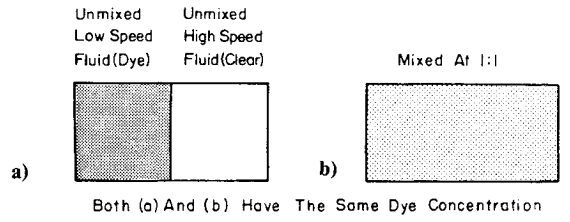

Fig. 9 Problem of probe finite sampling volume.

figure represents the visual thickness of the layer. Note the presence of unmixed low-speed fluid ($\xi = 0$) on the high-speed side ($y > 0$) and unmixed high-speed fluid ($\xi = 1$) on the low-speed edge ($y < 0$) of the layer. These time traces and also Fig. 6 show no evidence of a linear mean composition across a single vortex observed in gaseous layers.[1,5] The probability density function (pdf) of the composition field $p(\xi,y)$ was calculated from a long contiguous time series corresponding to the passage of approximately 100 structures and is shown in Fig. 8. The lateral composition uniformity, indicated qualitatively in Fig. 6, is confirmed by these data.

The most significant feature is that the apparent functional form of the mixed fluid pdf changes very little across the mixing layer (Fig. 8). This means that a given mixed fluid composition has roughly the same probability, relative to other mixed fluid compositions, of being observed regardless of position in the layer. Therefore, to the first order, we may think of the mixing layer as composed of structures filled with mixed fluid of a spatially uniform range of compositions. The absolute mixed fluid probability, at a given lateral point, is then proportional to the fraction of time that the observer spends inside the structures.

Another notable feature is that the mixed fluid composition is asymmetric and biased toward the high-speed fluid, implying that the entrainment into the layer is also asymmetric in favor of the high-speed fluid. This issue will be discussed in the following subsection.

Calculated Results and the Effect of Resolution

The present study of mixing in the shear layer yields an upper bound to the actual molecular mixing, which is pertinent to chemically reacting applications. This is a consequence of the fact that the measurement sampling volume, as determined by the resolution characteristics of the measuring apparatus, is larger than the smallest mixing (diffusion) scales. As an example, the smallest mixing scale in the high Reynolds number case has been estimated[8,10] to be about 1 μm, which is almost three orders of magnitude smaller than the resolution capability of the present measurement. This leads to an ambiguity that is illustrated in Fig. 9. Within the resolution volume of the measurement device, shown here symbolically by a rectangle, it is impossible to determine whether the two fluids are mixed or not. While we could make sound statements about mixing and concentration fluctuations down to the resolution scale of the measuring device, the only piece of information about the inside of this volume is the *average* concentration. It should be noted that the resolution difficulty described above is not limited to the present experiment, but also may affect any experiment that uses the passive scalar technique to measure molecular mixing (e.g., Refs. 1, 2, 4, and 22). See Ref. 10 for more discussion of resolution.

The pdf of the composition field, shown in Fig. 8, can be used to calculate the transverse profiles of some quantities of interest [see Eqs. (10-13)]. In order to investigate the effect of resolution on the results, the measurements above the mixing transition were repeated with the temporal resolution of the measurement degraded tenfold. This was done by increasing the array scan time from 0.8 to 8.0 ms. Results are reported below for both scan times.

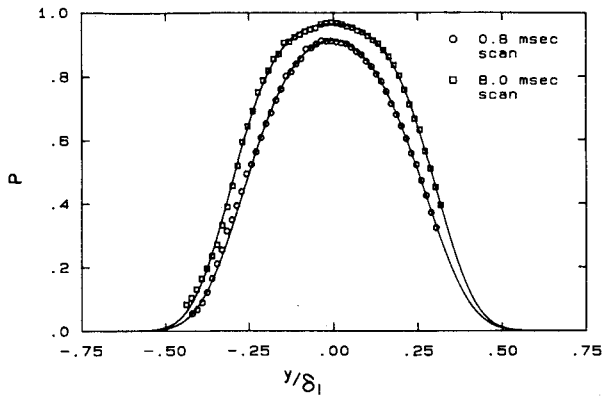

a) Total mixed fluid probability $P(y)$.

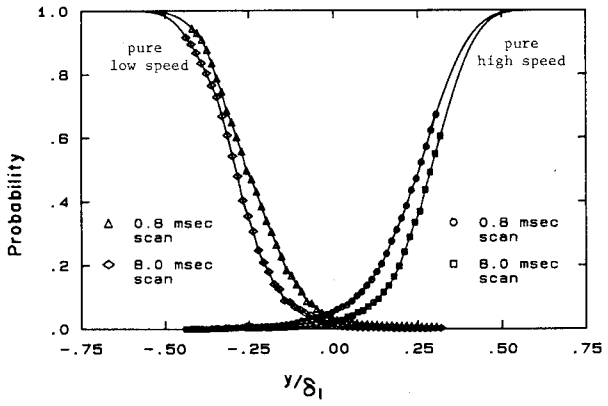

b) Probability of finding pure low- and high-speed fluids.

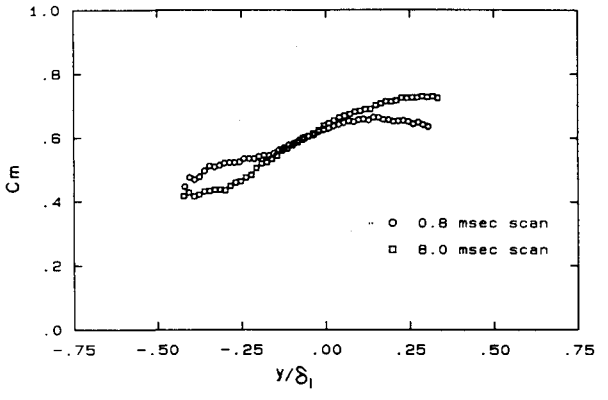

c) Average mixed fluid concentration $C_m(y)$.

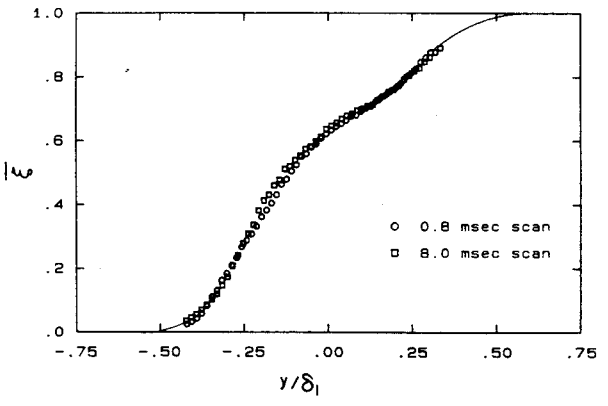

d) Average high-speed fluid concentration $\bar{\xi}(y)$.

Fig. 10 Calculated transverse profiles above the mixing transition.

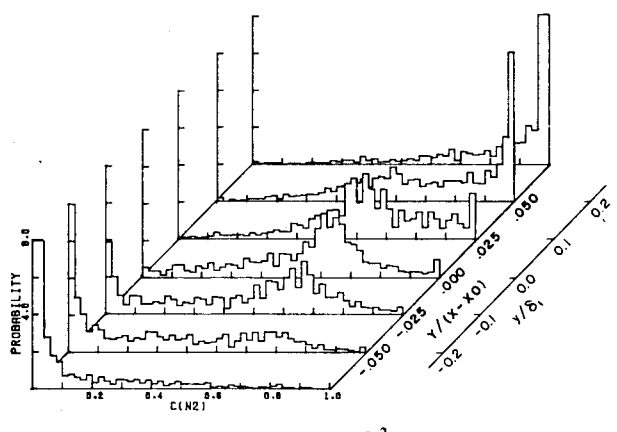

a) pdf from Konrad.[2]

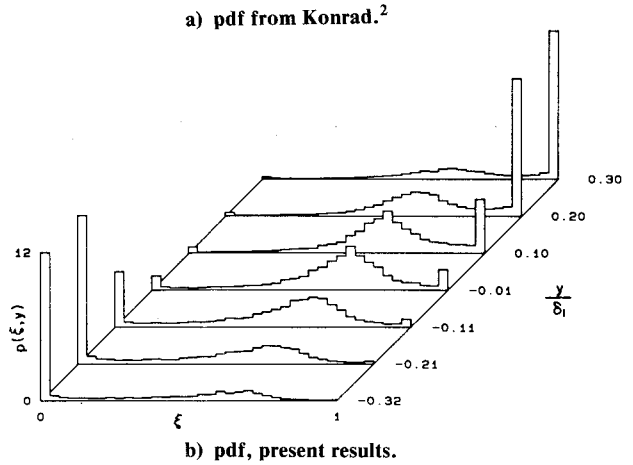

b) pdf, present results.

Fig. 11 Comparison of measured pdf with Konrad.[2]

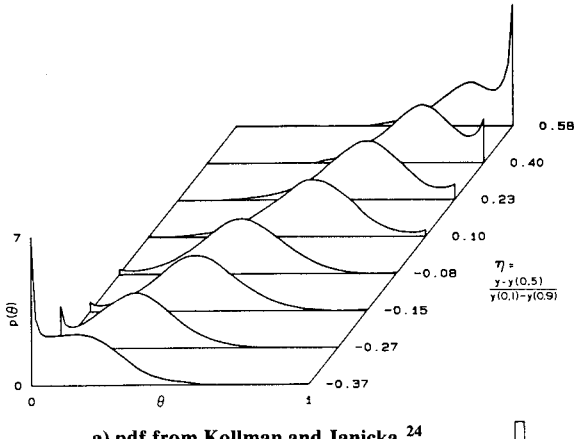

a) pdf from Kollman and Janicka.[24]

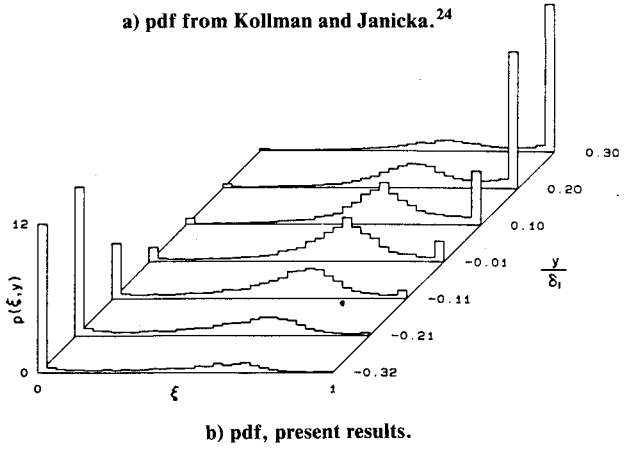

b) pdf, present results.

Fig. 12 Comparison of measured pdf with calculations of Kollmann and Janicka.[24]

The total probability of finding mixed fluid $P(y)$ [see Eq. (11)] is shown in Fig. 10a. Note that the probability of finding unmixed fluid is never zero, even in the center of the layer. The effect of lowering the resolution is to increase $P(y)$ everywhere in the layer indicating more mixed fluid. The increase of $P(y)$ is accomplished at the expense of lowering the probabilities of finding pure low- and high-speed fluids (see Fig. 10b). As Fig. 10c illustrates, the average mixed fluid concentration C_m for the 0.8 ms scan shows little variation across the layer, consistent with the transverse uniformity of the pdf's in Fig. 8. The variations of C_m across the layer increases when the resolution is degraded, causing an increase of mixed fluid concentration on the high-speed side ($y>0$) and a decrease on the low-speed side ($y<0$). It is interesting to note that the lack of adequate resolution seems to have changed the measured C_m profile in a direction that is qualitatively similar to what might be expected from an enhanced molecular diffusion process. The average concentration profile $\bar{\xi}(y)$, displayed in Fig. 10d, is not affected by a change in resolution, since it is based on the measurement of the *average* dye concentration. The peculiar shape of this profile, which is characterized by three inflection points, has been observed previously.[1,2,18,20] Fiedler[1] has concluded that the shape of this profile suggests a transport mechanism in which large-scale motion plays an important part.

That the lack of adequate resolution would give results indicating a higher degree of mixing is not new and was expected. However, these results also suggest that the resolution problem can lead to a measurement indicating a composition field that is less uniform across the layer than it really is (e.g., see the C_m profile in Fig. 10c). It is not clear how measured results at two different resolution levels, such as those presented in Fig. 10, can be extrapolated to the limit of "perfect" resolution. Such an extrapolation would in principle depend on the spectral characteristics of the composition fluctuations, which are not known a priori. In addition, one might expect that a resolution adequate to reproduce one quantity, e.g., the $C_m(y)$ profile, may not necessarily be adequate for the measurement of another, e.g., the $P(y)$ profile. For example, if the resolution volume happens to contain unmixed volumes of the fluids from the two freestreams at the proper ratio, the measured value of C_m would be correct, but not the value of P.

It was mentioned earlier that the composition of the mixed fluid is asymmetric and biased toward the high-speed fluid (see Fig. 8). Using Eq. (13) and the pdf's of Fig. 8, the average concentration of the mixed fluid for the whole layer C_M was calculated to be 0.60, indicating a mixture of 1.5 parts of high-speed to 1 part of low-speed fluids. If the notion of entrainment limited mixing above the mixing transition is correct, to the extent that the composition of the mixed fluid is determined by the amounts entrained from the two sides, we would conclude that the entrainment ratio E equals 1.5 in this case. This value is to be compared with the previously suggested[2,21] value of 1.3 for the velocity ratio used in this experiment.

Comparisons

Figure 10(a) shows that there is at least 10% probability of observing unmixed fluid in the center of the liquid mixing layer. This is higher than the value of 6% reported for gaseous layers at comparable Reynolds numbers.[1,2] The average mixed fluid concentration C_m (see Fig. 10c) is compared with the equivalent quantity measured in a gaseous layer by Fiedler (see Fig. 15 of Ref. 1). Our results show that the variation of this quantity across the layer is considerably less in the liquid than in the gas case. This implies that the mixed fluid composition in a liquid mixing layer may be more uniform laterally than that in the gaseous layer.

The general structure of the pdf of the mixed fluid composition that has been presented here for a liquid shear layer is similar to that measured in a gaseous layer by Konrad[2] (see Fig. 11). These results are in disagreement, however, with the measurements of the temperature pdf in a gaseous mixing layer by Batt[22] and the recent theoretical calculations of Pope[23] and Kollmann and Janicka.[24] The results of these calculations, both of which make use of a gradient diffusion model for turbulent transport, compare well with the temperature pdf of Batt. It would be expected that these calculations would also be applicable to the present case of a liquid, since they do not explicitly depend on the mass diffusion coefficient or, in nondimensional form, on the Schmidt number.

A comparison between the pdf calculated by Kollmann and Janicka[24] and the present results is shown in Fig. 12. These two suggest different mechanisms for turbulent transport and mixing. The calculated pdf's (Fig. 12a) change from point to point across the mixing layer and are more or less centered around the local mean at each location, whereas the form of the pdf's measured here (Fig. 12b) remains nearly the same all across the transverse extent of the layer. Note, for example, the trend of the peaks in the calculations, as opposed to their relatively fixed position in the measurements. Our results indicate that the processes of turbulent transport and mixing, in this flow, are not adequately described by the commonly used models of these processes. Comparison with the findings of Pope[23] leads to the same conclusions.

The results presented above suggest that a fluid element in the liquid mixing layer is found in one of three types of fluids: unmixed high-speed fluid, unmixed low-speed fluid, and mixed fluid at a composition whose pdf is essentially uniform across the layer. This description of fluid states in the turbulent mixing layer is qualitatively similar to that of Broadwell and Breidenthal[25] applied to the case of a liquid (high Schmidt number), with the exception that they represent the mixed fluid concentration at any point by a single value (delta function pdf). The description above is not limited to the flow Reynolds number presented in this paper and is consistent with the results of chemically reacting experiments at higher Reynolds numbers.[10]

Conclusions

The results presented show that the initial roll-up of the vortical structures in the mixing layer is not symmetric in the lateral direction and is such that a large excess of high-speed fluid is entrapped in the cores. Above the mixing transition, the composition of the mixed fluid is found to be essentially uniform across the width of the shear layer. It is asymmetric and biased toward the high-speed fluid, implying that the entrainment into the fully developed shear layer is also asymmetric. In the case of the high Schmidt number investigated here (water), the probability of finding unmixed fluid is never zero, even in the center of the layer, and it is higher than what has been measured in the gaseous case. This implies that the Schmidt number is an important parameter in turbulent mixing of high Reynolds number flows. The evidence suggests that the mixed fluid composition is more uniform across a liquid shear layer than that in the gaseous layer. Results show that the lack of adequate resolution of the measurement apparatus can indicate a composition field for the mixed fluid that is less uniform across the layer than it really is. Comparison with recent theoretical calculations indicates that the process of turbulent transport and mixing, in the case of the mixing layer, are not adequately described in these models. The fluid composition in the mixing layer, suggested by the present results, is in qualitative agreement with many aspects of the theoretical model of Broadwell and Breidenthal.

Acknowledgments

We would like to acknowledge the valuable contributions of Drs. D. B. Lang, and F. A. Roberts during the course of this research. This work was supported by the Air Force Office of Scientific Research, Contracts F44620-76-C-0046 and F49620-79-C-0159 and Grant AFOSR-83-0213.

References

[1]Fiedler, H. E., "Transport of Heat Across a Plane Turbulent Mixing Layer," *Advances in Geophysics*, Vol. 18A, 1974, pp. 93-109.

[2]Konrad, J. H., "An Experimental Investigation of Mixing in Two-Dimensional Turbulent Shear Flows with Applications to Diffusion-Limited Chemical Reactions," Project SQUID Tech. Rept. CIT-8-PU, 1976.

[3]Wallace, A. K., "Experimental Investigation of the Effects of Chemical Heat Release in the Reacting Turbulent Plane Shear Layer," Ph.D. Thesis, The University of Adelaide, Adelaide, Australia, 1981.

[4]Brown, J. L., "Heterogeneous Turbulent Mixing Layer Investigations Utilizing a 2-D 2-color Laser Doppler Anemometer and a Concentration Probe," Ph.D. Thesis, University of Missouri, Columbia, 1978.

[5]Mungal, M. G., "Experiments on Mixing and Combustion with Low Heat Release in a Turbulent Shear Flow," Ph.D. Thesis, California Institute of Technology, Pasadena, 1983; also *Journal of Fluid Mechanics*, Vol. 148, 1984, pp. 349-382.

[6]Mungal, M. G., Dimotakis, P. E., and Broadwell, J. E., "Turbulent Mixing and Combustion in a Reacting Shear Layer," *AIAA Journal*, Vol. 22, June 1984, pp. 797-800.

[7]Koochesfahani, M. M., Dimotakis, P. E., and Broadwell, J. E., "A 'Flip' Experiment in a Chemically Reacting Turbulent Mixing Layer," revised AIAA Paper 83-0475, Jan. 1983; also *AIAA Journal*, Vol. 23, Aug. 1985, pp. 1191-1194.

[8]Breidenthal, R. E., "A Chemically Reacting Turbulent Shear Layer," Ph.D. Thesis, California Institute of Technology, Pasadena, 1978; also "Structure in Turbulent Mixing Layer and Wakes Using a Chemical Reaction," *Journal of Fluid Mechanics*, Vol. 109, 1981, pp. 1-24.

[9]Bernal, L. P., Breidenthal, R. E., Brown, G. L., Konrad, J. H., and Roshko, A., "On the Development of Three-Dimensional Small Scales in Turbulent Mixing Layers," *Turbulent Shear Flows 2, Second International Symposium on Turbulent Shear Flows*, July 1979, Springer-Verlag, New York, pp. 305-313.

[10]Koochesfahani, M. M., "Experiments on Turbulent Mixing and Chemical Reactions in a Liquid Mixing Layer," Ph.D. Thesis, California Institute of Technology, Pasadena, 1984.

[11]Bilger, R. W., "Turbulent Flows with Nonpremixed Reactants," *Turbulent Reacting Flows*, edited by P. A. Libby and F. A. Williams, *Topics in Applied Physics*, Vol. 44, Springer-Verlag, New York, pp. 65-113.

[12]Freymuth, P., "On Transition in a Separated Laminar Boundary Layer," *Journal of Fluid Mechanics*, Vol. 25, Pt. 4, 1966, pp. 683-704.

[13]Rockwell, D. O., "External Excitation of Planar Jets," *Journal of Applied Mechanics*, Vol. 39, No. 4, Dec. 1972, pp. 883-890.

[14]Corcos, G. M. and Sherman, F. S., "Vorticity Concentration and the Dynamics of Unstable Free Shear Layers," *Journal of Fluid Mechanics*, Vol. 73, Pt. 2, 1976, pp. 241-264.

[15]Jimenez, J., "On the Visual Growth of a Turbulent Mixing Layer," *Journal of Fluid Mechanics*, Vol. 96, Pt. 3, 1980, pp. 447-460.

[16]Brown, G. L. and Roshko, A., "The Effect of Density Differences on the Turbulent Mixing Layer," *Turbulent Shear Flows*, AGARD CP-93, 1971, pp. 23.1-23.12.

[17]Winant, C. D. and Browand, F. K., "Vortex Pairing: The Mechanism of Turbulent Mixing-Layer Growth at Moderate Reynolds Number," *Journal of Fluid Mechanics*, Vol. 63, Pt. 2, 1974, pp. 237-255.

[18]Brown, G. L. and Roshko, A., "On Density Effects and Large Structure in Turbulent Mixing Layers," *Journal of Fluid Mechanics*, Vol. 64, Pt. 4, 1974, pp. 775-816.

[19]Wygnanski, I., Oster, D., and Fiedler, H., "A Forced, Plane, Turbulent Mixing-Layer: A Challenge for the Predictor," *Turbulent Shear Flows 2, Second International Symposium on Turbulent Shear Flows*, July 1979, Springer-Verlag, New York, pp. 314-326.

[20]Rajagopalan, S. and Antonia, R. A., "Properties of the Large Structure in a Slightly Heated Turbulent Mixing Layer of a Plane Jet," *Journal of Fluid Mechanics*, Vol. 105, 1981, pp. 261-281.

[21]Dimotakis, P. E., "Two-Dimensional Shear Layer Entrainment," revised AIAA Paper 84-0368, Jan. 1984; also *AIAA Journal*, to be published.

[22]Batt, R. G., "Turbulent Mixing of Passive and Chemically Reacting Species in a Low-Speed Shear Layer, *Journal of Fluid Mechanics*, Vol. 82, 1977, pp. 53-95.

[23]Pope, S. B., "A Monte Carlo Method for the PDF Equations of Turbulent Reactive Flow," *Combustion Science and Technology*, Vol. 25, 1981, pp. 159-174.

[24]Kollmann, W. and Janicka, J., "The Probability Density Function of a Passive Scalar in Turbulent Shear Flows," *The Physics of Fluids*, Vol. 25, No. 10, 1982, pp. 1755-1769.

[25]Broadwell, J. E. and Breidenthal, R. E., "A Simple Model of Mixing and Chemical Reaction in a Turbulent Shear Layer," *Journal of Fluid Mechanics*, Vol. 125, 1982, pp. 397-410.